V2X Sidelink Localization of Connected Automated Vehicles

Nicolò Decarli, *Member, IEEE*, Anna Guerra, *Member, IEEE*, Caterina Giovannetti, *Student Member, IEEE*, Francesco Guidi, *Member, IEEE*, and Barbara M. Masini, *Senior Member, IEEE*

***Abstract*— Future automated driving relies on two pillars, *(i)* ultra-low-latency and reliable communications, and *(ii)* accurate positioning information. In particular, the knowledge of vehicle positions is becoming fundamental with the increase of the automation level, allowing autonomous navigation of the environment. Today's positioning techniques cannot provide the accuracy, robustness, and latency required for stringent applications, like platooning, where vehicles are expected to travel at extremely short distances. In this paper, we leverage vehicle-to-everything (V2X) sidelink communication for localization purposes, capitalizing on the near-field propagation attributes of signals generated utilizing high carrier frequencies and/or large antenna arrays. Consequently, a receiving vehicle can accurately determine the transmitting vehicle's location through V2X sidelink packet reception, obviating the need for supplementary reference nodes or stringent synchronization. Fundamental limits on localization accuracy are derived to characterize the positioning performance in vehicular contexts. A case study based on 5G new radio (NR) V2X sidelink shows how this technique is extremely promising and capable of providing high accuracy, low latency, high update rate, and high availability of position information in realistic vehicular scenarios.**

***Index Terms*— V2X sidelink, near-field localization, sidelink positioning, 5G NR-V2X, connected automated vehicles.**

I. Introduction

FUTURE automated driving and enhanced traffic experiences can be supported by advanced vehicle-to-everything (V2X) communication systems. The recent advances in V2X communication technologies enabled by the fifth generation (5G) new radio (NR) and flashed by the sixth generation (6G) will, in fact, lift vehicles to the next level of safety, comfort, and efficiency and will allow the underlying communication systems to face and solve new challenges, such as those provided by cooperative or remote driving scenarios that require ultra-low latency and high reliability. In addition, 5G NR-V2X communications should enable vehicles to *see through the eyes* of their neighbors in a distributed fashion, significantly extending the sensing range provided by devices, such as cameras, radio detection and ranging (RADAR), and light detection and ranging (LiDAR). The advent of 6G is expected to enhance localization and sensing capabilities into devices traditionally conceived for wireless communications only [1], [2], thus supporting a myriad of new applications based on the convergence of these three functionalities [3], [4], [5], [6], [7]. Thus, vehicles are envisioned as capable of determining their absolute and/or relative positions in the environment. It is worth saying that different V2X use cases foresee different requirements both in terms of communication and positioning [8]; for example, focusing on cooperative driving scenarios, the platooning application requires a communication latency lower than $10\,\mathrm{ms}$ and reliability of 99.99% for vehicles with high level of automation [9] and cm-level positioning accuracy [10], [11]. Indeed, there is still the need to design ad-hoc schemes to attain such challenging requirements [12].

In this work, we focus on cooperative driving scenarios as they represent one of the advanced scenarios foreseen by 5G NR-V2X [9], and we specifically address the platooning application since it summarizes most of the challenges to be faced. Classical radio localization techniques, such as global navigation satellite system (GNSS), are not available in all environments, such as tunnels or urban canyons, and they hardly satisfy the accuracy and latency requirements. For this reason, data fusion techniques [13] exploiting inertial sensors, time-of-flight (ToF) cameras and/or LiDAR [14], visible light communication (VLC) [15], [16], and RADAR sensors are typically considered, at the expense of an ad-hoc installation and, thus, extra costs. Moreover, since RADAR/LiDAR are passive technologies (i.e., relying on signal reflection), they only detect and localize a generic obstacle around a specific vehicle where they are installed, but they have no capability of identifying it as feasible when establishing a radio communication link between vehicles.

As an additional opportunity to gather positioning information, the exploitation of an onboard available V2X radio access technology could be considered, facilitated by interoperable standards expected to be diffused worldwide in the near future. Unfortunately, common radio localization techniques cannot be easily adapted to V2X communication systems, as they require either a tight synchronization between the transmitter and the receiver, which is unavailable, or the deployment of a dedicated localization infrastructure in addition to the

Manuscript received 14 February 2023; revised 22 June 2023; accepted 13 August 2023. Date of publication 9 October 2023; date of current version 19 December 2023. This work was supported in part by the European Union under the Italian National Recovery and Resilience Plan (NRRP) of NextGenerationEU, partnership on Telecommunications of the Future (RESTART program) under Grant PE00000001. An earlier and reduced version of this paper was presented at the Workshop on Near-Field Localization and Communication for 6G, IEEE International Conference on Communications (ICC), Rome, Italy, in June 2023. *(Corresponding author: Nicolò Decarli.)*

The authors are with the National Research Council, Institute of Electronics, Computer and Telecommunication Engineering (CNR-IEIIT), 40136 Bologna, Italy, and also with WiLab-CNIT, 40136 Bologna, Italy (e-mail: nicolo.decarli@cnr.it; anna.guerra@cnr.it; caterina.giovannetti@cnr.it; francesco.guidi@cnr.it; barbara.masini@cnr.it).

Color versions of one or more figures in this article are available at https://doi.org/10.1109/JSAC.2023.3322853.

Digital Object Identifier 10.1109/JSAC.2023.3322853

direct vehicle-to-vehicle communication exploiting sidelink, which is the pillar of V2X applications. Furthermore, time-difference-of-arrival (TDoA) and/or angle of arrival (AoA) measurements over cellular network [17], [18], [19], [20], [21] suffer from unreliability for providing the positioning information with the requested latency and accuracy in every operating condition [22].

In this paper, we propose exploiting V2X sidelink for relative localization of connected automated vehicles (CAVs) by addressing vehicles' ability to operate in the near-field region. In fact, 5G and beyond systems are likely to work in the near-field propagation regime [23], [24] due to adopting high frequency and/or large antenna arrays. This will offer the possibility to exploit the spherical wavefront for enhancing wireless localization at an unprecedented scale, without the need for a tight synchronization or for the deployment of an ad-hoc infrastructure [25], [26]. To this purpose, we derive the fundamental localization limits considering V2X sidelink in the near field, with the aim of understanding when the distance and the AoA estimates are sufficiently accurate and allow to directly locate another vehicle (i.e., relative localization). Then, we introduce the main characteristics of 5G NR-V2X sidelink, discussing how the proposed sidelink-enabled near-field localization can be implemented.

The main contributions can be summarized as follows.

- We provide a comprehensive discussion about V2X localization, and the advantages and disadvantages of different solutions, highlighting their possible implementations.
- We propose the adoption of near-field localization exploiting V2X sidelink. To this end, we derive the near-field fundamental positioning limits in order to assess the possibility of implementing this scheme. The proposed approach does not require a dedicated infrastructure and synchronization, which are the main limitations of other V2X localization techniques.
- We discuss how the proposed approach can be implemented by accounting for the 5G NR-V2X standard and its policies related to pilot schemes and resource allocation modes; an extensive simulation analysis in a realistic multi-vehicles scenario then assesses its performance showing the impact of the different parameters.

The rest of the paper is organized as follows. In Sec. II, radio positioning techniques tailored to vehicular scenarios are discussed. The proposed V2X sidelink near-field positioning technique is then presented in Sec. III together with its ultimate performance limits. Then, Sec. IV introduces the main characteristics of 5G NR-V2X sidelink in relationship with the implementation of the proposed technique, and numerical results are reported in Sec. V. Finally, conclusions are drawn in Sec. VI.

Notations and Definitions: Boldface lower-case letters are vectors (e.g., $\mathbf{x}$), whereas boldface capital letters are matrices (e.g., $\mathbf{H}$). Notation $h_{n,m} = [\mathbf{H}]_{nm}$ represents the (n,m)th element of matrix $\mathbf{H}$, and $\mathbf{H}^\top$ indicates the transpose applied to matrix $\mathbf{H}$. The notation $x \sim \mathcal{CN}\left(m, \sigma^2\right)$ indicates a complex circular symmetric Gaussian random variable with mean m and variance σ^2. The real part of a complex number z is $\Re\{z\}$ and $\mathrm{j} \triangleq \sqrt{-1}$.

II. Vehicular Communications and Localization

In this section, we discuss positioning techniques tailored to vehicular contexts. A specific emphasis is given to solutions based on the V2X *sidelink*, hence the direct communication between vehicles, considered as baseline for V2X applications [9], [27], [28].

A. V2X Communications and Use Cases

Direct V2X communication among user equipments (UEs), hence among vehicles, has been introduced by the Third Generation Partnership Project (3GPP) Release 14 (and later refined in Release 15) of the long term evolution (LTE) V2X standard and has the peculiarity of not relying on the cellular network. LTE V2X mainly supports awareness services similarly to ITS-G5 in Europe or IEEE 802.11p in the US. By broadcasting awareness messages, known as cooperative awareness messages (CAMs) in ITS-G5, a vehicle informs others about its actual status, such as position (e.g., from GNSS), speed, acceleration, and direction. 5G NR-V2X has been designed to complement LTE V2X to support advanced use cases and to enable higher automation levels [29] as defined by 3GPP Services and System Aspects (SA) Working Group 1 (SA1) [30], [31] and further developed by the 5G Automotive Association (5GAA) Working Group 1 [32]: vehicles platooning, advanced driving, and remote driving.

To satisfy the requirements of larger bandwidth for the advanced use cases, 5G NR-V2X sidelink was designed to operate in larger frequency ranges, that are *(i)* frequency range 1 (FR1) at $410\,\mathrm{MHz}$ - $7.125\,\mathrm{GHz}$ (sub-6 GHz), and *(ii)* frequency range 2 (FR2) at $24.25\,\mathrm{GHz}$ - $52.6\,\mathrm{GHz}$ (millimeter-wave (mmWave)). The maximum single user bandwidth in FR1 and FR2 is $100\,\mathrm{MHz}$ and $400\,\mathrm{MHz}$, respectively, against a maximum of $20\,\mathrm{MHz}$ in LTE-V2X, even if today available services work in a $10\,\mathrm{MHz}$ band at FR1. From the physical (PHY) layer point of view, 5G NR-V2X sidelink transmissions are based on cyclic prefix orthogonal frequency-division multiplexing (OFDM) (CP-OFDM).

Among the different applications, a particular interest is devoted to *vehicle platooning*. Platooning is intended as a dynamically formed group of vehicles traveling together at a generally constant speed and with extremely small inter-vehicle distance, thus capable of reducing dramatically fuel consumption. Periodic data exchange is required to ensure the correct functioning of the platoon, and, in this context, using sidelink can ensure the required low latency and high reliability for enabling extremely reduced inter-vehicle distances with a reasonable safety margin. Requirements are increasingly stringent as the level of vehicle automation increases.

B. V2X Localization

The mentioned V2X advanced use cases, like platooning, rely on the precise knowledge of the vehicles' positions. In fact, as an example, every vehicle in the platoon must quickly react if the relative distance with contiguous vehicles changes for any reason. Similarly, when overtaking, a precise location knowledge of nearby vehicles is mandatory for safely accomplishing the maneuver.

In general, any automated driving operation requires precise positioning and, in particular, the knowledge of the *relative* positions of the other vehicles in the environment with respect to the considered one. This is of paramount importance to avoid, for example, a collision. Therefore, in this context, the absolute position of vehicles is usually unnecessary [29]. In the rest of the paper, we consider the following terminology to distinguish among the vehicles involved in the positioning process:

1) The *automated vehicle (AV)*: the vehicle which needs to know the positions of the *neighbor vehicles* (see next definition) for its use (e.g., automated driving).
2) The *neighbor vehicles (NVs)*: the other vehicles in the surroundings of the AV (e.g., located within the communication range), whose relative positions must be estimated by the AV.

In this work, our goal is obtaining relative positioning information of NVs (2) at the AV (1) side. Of course, every vehicle in the scenario can simultaneously be AV and NV. The radio-based positioning process involves exchanging signals and measurements based on that [33]. When the position of a specific node is known, it is called *reference node* or *anchor*.

Localization techniques tailored to vehicular use cases, such as platooning, must provide [3]:

1) High *accuracy*: this is required when the inter-vehicle distance becomes very low and/or when the speed becomes very high. Differently, the accuracy requirement can be relaxed at large distances and low speeds.
2) High *availability*: positioning information must always be available, independently of the coverage of fixed networks or satellite constellations.
3) High *update rate*: position information must be updated several times per second to properly feed the control system (e.g., the automated driving engine).
4) Low *latency*: position information must be extremely up-to-date to enable fast reactions even in high-speed contexts.

In addition to the above-mentioned key performance indicators (KPIs), other goals should be targeted, for example:

- No need for an external anchor-based localization infrastructure rather than the AV itself. This, in turn, means that we only need relative positions of NVs w.r.t. the considered AV.
- No need for tight synchronization among vehicles and/or infrastructure, which could be only partially achievable.
- The exploitation of the same signals used for communication, thus ensuring the minimum spectrum consumption.

In the following, we discuss traditional localization techniques in vehicular contexts in light of the above-mentioned characteristics.

1) GNSS-Based Localization: Satellite-based localization allows obtaining the absolute position of each vehicle in the scenario. Satellites are reference nodes for positioning purposes. The position is available locally for each vehicle. Thus, since the position of NVs is required at the AV side, the exchange of information with V2X communication signals is required, leading to unavoidable additional latency. Moreover, the standard GNSS accuracy is too low for stringent requirements such as platooning applications.[1] Finally, GNSS positioning has limited availability, and it is precluded in urban canyons, road tunnels, covered parking sites, etc., thus requiring other complementary solutions.

2) UWB-Based Localization: Nowadays, ultra-wide bandwidth (UWB) is the leading radio technology capable of providing reliable and high-accuracy localization [34]. This is mainly due to the large bandwidth, translating in high-accuracy time-of-arrival (ToA) estimation capability even in the presence of strong multipath thanks to the exploitation of impulse-based radios [35]. UWB is a short-distance communication technology, so localization of vehicles based on it would be possible only assuming the availability of this radio interface at the vehicles' side. Two main localization schemes are foreseen: *(i)* two-way ranging (TWR), and *(ii)* TDoA. For TWR, no synchronization is required among vehicles. The AV, by measuring the distance (ranging) with respect to some NVs from the round-trip time, can determine its own position. Of course, this requires the knowledge of the NVs positions, acting as reference nodes. If this is not available (since it is itself the object of the positioning process), cooperative techniques could be considered, requiring the exchange of a large number of packets until convergence (i.e., estimation of the positions of all the nodes, AV and NVs) is achieved [36], [37]. This approach makes latency explode, thus being unfeasible for real-time operations. Moreover, the continuous changes of the vehicle positions during the time (highly dynamic environment) make every cooperative technique extremely challenging. The same issue applies to TDoA-based solutions, which substantially decrease the number of packets that have to be exchanged (lower latency) at the expense of the need for tight synchronization. Recently, UWB-TDoA solutions with multiple reference nodes on the same vehicle (e.g., at its corners) have been proposed [38]. The presence of multiple reference nodes on the same vehicle (i.e., the AV) simplifies the synchronization and makes the positioning of a transmitting NV possible with a receiving-only scheme using TDoA (low complexity and low latency). Unfortunately, this scheme leads to large geometric dilution of precision (GDOP) conditions since localization is realized outside the perimeter of anchors, so high accuracy is possible only at relatively low distances. However, impulse-based UWB solutions are not compatible with standard V2X communication systems such as 5G NR, making their applicability limited in practical contexts.

3) Network-Based Localization: Exploiting the 5G network is foreseen as an enabler of positioning [17], [18]. Network-based solutions can leverage to TDoA and AoA information by exploiting antenna arrays. Moreover, downlink and uplink signals can be used. The network, e.g., the road side units (RSUs), act as reference nodes for positioning purposes. When exploiting uplink signals, positioning is realized by the network; then, the position information must be transferred to the AV to build the relative positions of NVs necessary for automated driving. As for GNSS-based techniques, this leads to additional latency and propagation of errors [29]. Differently, if downlink signals

[1]Eventually, differential-GNSS techniques could be considered at the expense of increased cost and complexity.

are considered, each node (AV or NV) determines its own position, as for GNSS, thus requiring information exchange again at the expense of the latency. Of course, this requires the knowledge of the reference node positions (e.g., RSUs). The main advantage of network-based techniques is exploiting the same signals already adopted for communication, thus avoiding additional spectral occupation with wide bandwidth signals. On the other side, the limited bandwidth makes TDoA-based solution incapable of providing the required level of accuracy. Moreover, if 5G gNodeBs are in non-line-of-sight (NLOS) conditions with respect to the vehicles, both AoA and TDoA solutions could be severely impacted. The main disadvantage of network-based localization is the need for network coverage, with multiple gNodeBs to properly fuse AoA measurements and/or compute TDoA measurements, which cannot always be guaranteed.

4) V2X Sidelink-Based Localization: Positioning techniques based on sidelink measurements may complement GNSS-based and network-based positioning even in out-of-coverage scenarios [21], [39], [40], [41]. When considering sidelink positioning, if measurements from multiple vehicles must be fused (e.g., ToA or AoA information), the movement of all the nodes involved, including the reference ones, makes the process challenging. As for UWB positioning, cooperative solutions could be considered [42], [43], [44], [45], but at the expense of complexity and latency. Moreover, the limited bandwidth could make ToA estimation over sidelink not accurate, especially in the presence of multipath. Recently a proposal of using a receiving-only AV equipped with more than one antenna array was made [46], thus exploiting the large dimensions of the vehicle for collecting multiple AoA and TDoA measurements and enabling the localization of a transmitting-only NV. Such a solution allows for achieving the requirements listed in the previous section at the expense of additional hardware complexity. In light of the potential offered by the sidelink interface, in the following section, a novel sidelink-based positioning technique will be proposed, based on the exploitation of the near-field propagation characteristics of the radio signals [23], when electrically large antenna arrays are considered; this allows avoiding synchronization, cooperation among vehicles, yet providing high accuracy also with narrowband signals.

III. V2X Sidelink Near-Field Localization

In this section, we introduce the proposed solution for the relative localization of vehicles based on near-field propagation, exploiting V2X sidelink communications.

It is well-known that an antenna array can be used for estimating the AoA of a received signal (bearing estimation problem [47]). In fact, in classical operating conditions, the signal sent by the transmitter reaches the array with a wavefront that can be approximated as planar, thus producing a linear phase difference between the elements of the array, which is a function of the impinging angle [47]. However, with increasing array sizes and high operating frequencies, the assumption of a planar wavefront on the receiving array may not be fulfilled. The wavefront produced by an antenna of maximum size D transmitting at frequency f_c may be considered approximately planar if the observation point is located at a distance larger than the Fraunhofer distance, conventionally defined as

$$d_F = \frac{2D^2}{\lambda} \tag{1}$$

where $\lambda = c/f_c$ indicates the wavelength, f_c is the carrier frequency, and c is the speed of light. Considering the dual problem related to AoA estimation, the wavefront generated from a point source at a distance d from the receiving antenna array of size D can be considered approximately planar if the transmitter is located at $d > d_F$. When such a condition does not hold, due, for example, to the use of a large receiving array, the curvature of the wavefront impinging on the array must be considered [48]. In the last decade, it has been demonstrated how, in this case, richer information concerning the position of the transmitting source can be obtained, thus enabling direct positioning using a single array (i.e., single anchor localization) [49], [50]. This is exactly the desired operating setup for sidelink positioning to enable the localization of a single-antenna transmitting vehicle (i.e., a NV, sending its packet through the V2X sidelink interface), with the processing operated exploiting a large array at the receiving vehicle (i.e., the AV). Considering a typical vehicle size and assuming a large array deployed along the vehicle transverse direction (e.g., $D = 1.7\,\mathrm{m}$ for a car and $D = 2.2\,\mathrm{m}$ for a truck), the Fraunhofer distance results in $d_F = 113\,\mathrm{m}$ and $d_F = 190\,\mathrm{m}$ for the two vehicles' sizes, respectively, assuming a carrier frequency $f_c = 5.9\,\mathrm{GHz}$ as for today's sidelink communication (i.e., $\lambda \approx 5\,\mathrm{cm}$). Considering the same array size and assuming to work at mmWave (e.g., $f_c = 28\,\mathrm{GHz}$), the Fraunhofer distance results in $d_F = 539\,\mathrm{m}$ and $d_F = 903\,\mathrm{m}$, respectively. Motivated by these considerations and focusing on use cases such as platooning scenarios, where it is fundamental to infer the position of close vehicles with relative distance typically much smaller than the Fraunhofer distance, we propose near-field localization using V2X sidelink.

In the following, we consider 2D positioning since we can assume vehicles lying on the same plane with a very good approximation, and the use of a large uniform linear array (ULA) along the vehicle transverse direction (e.g., over the truck/automobile roof or nose) for relative localization at the AV side of the non-synchronized nearby NVs transmitting packets over the V2X sidelink interface.

A. Signal Model

We now describe the signal model we adopt to realize near-field localization among vehicles. Consider a generic OFDM signal, with a total number N of subcarriers and a number M of OFDM symbols for the transmission of a sidelink data packet. In particular, the m-th transmitted OFDM symbol, in complex baseband, can be written as

$$s_m(t) = \sum_{n=0}^{N-1} \sqrt{P_n}\, x_{n,m} e^{\mathrm{j}2\pi n \Delta f t}\, \mathrm{rect}\left(\frac{t - mT_{\mathrm{sym}}}{T_{\mathrm{sym}}}\right) \tag{2}$$

where $P_n = P \triangleq P_T/N, \forall n$, is the power allocated to each subcarrier, P_T is the total transmit power, and $x_{n,m}$ is the data symbol transmitted in the n-th subcarrier of the m-th symbol with $\mathbb{E}\left\{|x_{n,m}|^2\right\} = 1$. The symbol time is $T_{\mathrm{sym}} = T + T_{\mathrm{cp}}$

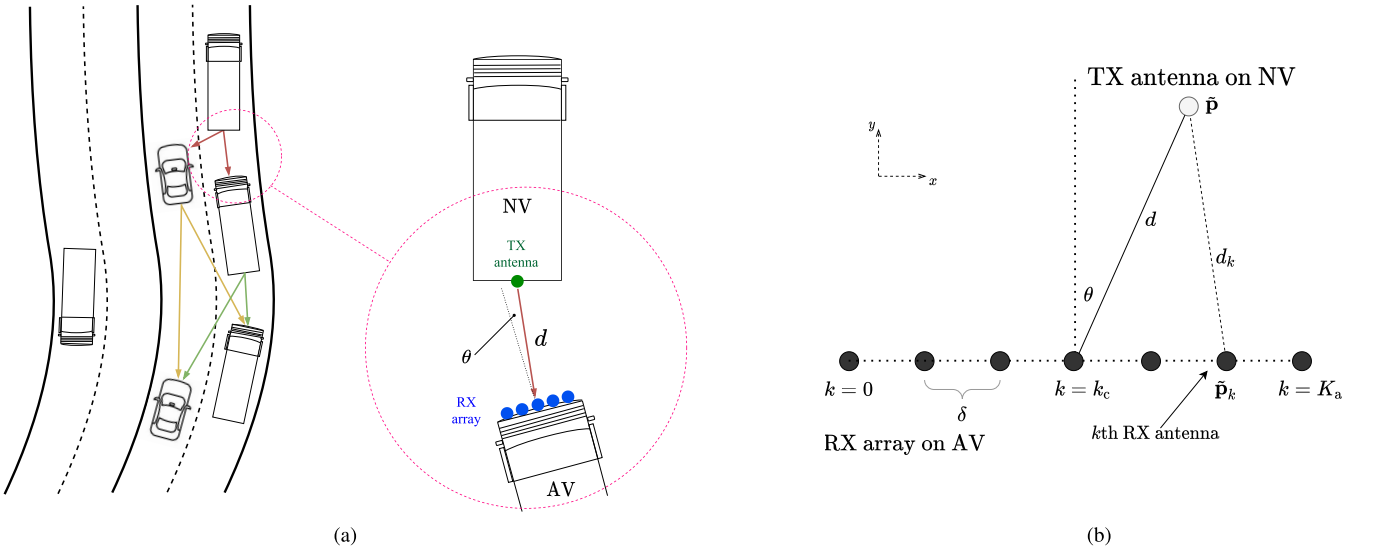

(a) (b)

Fig. 1. (a) Example of vehicular scenario with multiple vehicles communicating through the V2X sidelink interface. Vehicles can also realize platoons by traveling at close distances to each other and at a constant speed. (b) The geometry of the scenario with a transmitting antenna (e.g., on the back side of a truck assumed as a neighbor vehicle - NV) and a large uniform linear array (ULA) of receiving antennas (e.g., on the front side of a truck assumed as an automated vehicle - AV). Center of the reference system on the central element ($k = k_{\rm c}$) of the receiving array on the AV.

where $T_{\rm cp}$ stands for the cyclic prefix duration and $T = 1/\Delta f$, with Δf indicating the subcarrier spacing (SCS). The pass-band signal transmitted by the vehicle (here assumed a generic NV), whose transmitting antenna is in position $\tilde{\mathbf{p}} = [x, y]^\top$, is

$$\tilde{s}(t) = \Re\left\{\sum_{m=0}^{M-1} s_m(t) e^{\mathrm{j}2\pi f_{\rm c} t}\right\}. \tag{3}$$

The signal is then received by another vehicle (here assumed the AV), aiming at estimating the position $\tilde{\mathbf{p}}$ using a large ULA. We assume the receiving vehicle is not synchronized (in time and phase) with the NV. The receiving ULA is assumed oriented along the x direction (see Fig. 1) and composed of $K_{\rm a}$ antennas spaced of $\delta = \lambda/2$ to make mutual coupling among the antenna elements negligible. Without loss of generality, let us assume $K_{\rm a}$ to be odd, so that the element of index $k_{\rm c} = (K_{\rm a}+1)/2$ is the central one. Denote with $\tilde{\mathbf{p}}_k = [x_k, y_k]^\top$ the position of the k-th receiving antenna and assume the origin of the reference system in correspondence of the central antenna element so that $y_k = 0, \forall k$, and $x_{k_{\rm c}} = 0$. Let us now consider, for convenience, a polar coordinate system. In this case, we can write the position of the transmitting vehicle as $\mathbf{p} = [\theta, d]^\top$ where θ denotes the angle with respect to the boresight direction of the receiving ULA (i.e., the AoA of the received signal at the AV), and d denotes the distance between the NV and the central element of the receiving ULA at the AV, that is

$$d = \sqrt{x^2 + y^2}, \quad \theta = \operatorname{atan}\left(\frac{x}{y}\right) \tag{4}$$

where $\operatorname{atan}(\cdot)$ is the four-quadrant inverse tangent. We denote with d_k the distance between the transmitting antenna and the k-th receiving antenna that can be expressed as

$$d_k = \|\tilde{\mathbf{p}} - \tilde{\mathbf{p}}_k\| = \sqrt{(x_k - x)^2 + y^2}. \tag{5}$$

We drop the dependence on the symbol in the sequel for notation simplicity. After standard cyclic prefix removal and FFT processing, the received signal at the k-th antenna is

$$y_{n,k} = \sqrt{P}\, x_n h_{n,k}\, e^{-\mathrm{j}2\pi f_n \tau_k} e^{\mathrm{j}2\pi f_n t_0} e^{\mathrm{j}\varphi_0} + z_{n,k} \tag{6}$$

where $f_n \triangleq f_{\rm c} + \left(n - \frac{N-1}{2}\right)\Delta f$ is the frequency associated with the n-th subcarrier, $\tau_k = d_k/c$ is the propagation time from the source to the k-th ULA antenna, t_0 and φ_0 account for the time and phase synchronization mismatches respectively, and $h_{n,k}$ is the channel gain. The term $z_{n,k}$ denotes the additive white Gaussian noise (AWGN), with $z_{n,k} \sim \mathcal{CN}(0, \sigma^2)$ and $\sigma^2 = k_{\rm B} T_0 F \Delta f$, being $k_{\rm B}$ the Boltzmann constant, T_0 the reference temperature, and F the receiver noise figure. Let us consider the channel gain equal for all the antennas, which is reasonable for the practical size of the receiving ULA, and small bandwidth so that we can write $h_{n,k} = h, \forall n, k$.

Among the MN data symbols transmitted, a subset comprises pilot symbols (thus known at the receiver), usually exploited for channel estimation. Considering the transmission of pilots data in $M_{\rm p}$ OFDM symbols out of M and $N_{\rm p}$ subcarriers out of N, we can assume $x_{n,m} = 1, \forall\, n \in \mathcal{N}_{\rm p}, m \in \mathcal{M}_{\rm p}$, where we have defined with $\mathcal{N}_{\rm p}$ ($\mathcal{M}_{\rm p}$) the set of indexes n (m) relative to subcarriers (OFDM symbols) occupied by pilots, with a cardinality $|\mathcal{N}_{\rm p}| = N_{\rm p}$ ($|\mathcal{M}_{\rm p}| = M_{\rm p}$). These pilots will also be considered for the transmitting vehicle's localization.

B. Bound on the Localization Accuracy

In this section, starting from the above-discussed signal model, we want to evaluate the localization performance limits when considering near-field signal characteristics. The goal is to obtain an estimate $\widehat{\mathbf{p}} = [\,\widehat{\theta}, \widehat{d}\,]^\top$ of the transmitting NV vehicle position $\mathbf{p} = [\theta, d]^\top$, without requiring synchronization among vehicles.[2]

[2]Notice that this is not possibile with a standard ULA, since only information concerning the AoA can be retrieved by the impinging planar wavefront on the receiving ULA.

1) Observation Model: Considering K_a antennas and N_p pilots, the AV can collect $N_\mathrm{p} \times K_\mathrm{a}$ phase observations $\phi_{l,k}$, $l = 0, \dots N_\mathrm{p} - 1$, $k = 0, \dots K_\mathrm{a} - 1$, where

$$\phi_{l,k} = \xi_{l,k}(\mathbf{p}) \bmod 2\pi + \omega_{l,k} \tag{7}$$

with mod being the modulo operator, so that $a \bmod b$ returns the remainder after division between a and b, and with, according to (6),

$$\xi_{l,k}(\mathbf{p}) = -\frac{2\pi}{\lambda_l} d_k(\mathbf{p}) + 2\pi f_l t_0 + \varphi_0 \tag{8}$$

and $\lambda_l = c/f_l$, $f_l = f_\mathrm{c} + \left(n(l) - \frac{N-1}{2}\right)\Delta f$, where $n(l)$ indicates the index of the subcarrier used as pilot from the set $\mathcal{N}_\mathrm{p}$ indexed by l. We made explicit the dependence from $\mathbf{p}$ of d_k and $\xi_{l,k}$ using the notation $d_k(\mathbf{p})$ and $\xi_{l,k}(\mathbf{p})$, respectively. The phase noise in (8), namely $\omega_{l,k}$, can be characterized according to the Cramér-Rao Lower Bound (CRLB) for phase estimates.[3] By assuming averaging among M_p observations for each subcarrier,[4] we have $\omega_{l,k} \sim \mathcal{N}(0, \sigma_\phi^2)$, with $\sigma_\phi^2 = \eta/(2M_\mathrm{p}\mathsf{SNR})$ where $\eta \geq 1$ accounts for non-ideal phase estimates at the receiver side and where SNR is the signal-to-noise ratio (SNR) defined as $\mathsf{SNR} = Ph^2/\sigma^2$.

In order to make the receiver independent of the clock and phase synchronization mismatch, we consider differential phase observations with respect to the central antenna of the receiving array (i.e., reference antenna), that is

$$\Delta\phi_{l,k} = \quad \phi_{l,k} - \phi_{l,k_\mathrm{c}} = \Delta\xi_{l,k}(\mathbf{p}) \bmod 2\pi + \tilde{\omega}_{l,k} \tag{9}$$

with $\tilde{\omega}_{l,k} \sim \mathcal{N}(0, 2\sigma_\phi^2)$ and

$$\Delta\xi_{l,k}(\mathbf{p}) = -\frac{2\pi}{\lambda_l}\left(d_k(\mathbf{p}) - d\right) = -\frac{2\pi}{\lambda_l}\Delta d_k(\mathbf{p}) \tag{10}$$

where the term $\Delta d_k(\mathbf{p})$ denotes the distance-difference traveled by the signal to reach the k-th antenna of the ULA with respect to the central one. By using the geometrical relationship

$$d_k^2 = d^2 + x_k^2 - 2dx_k \cos\left(\frac{\pi}{2} - \theta\right) \tag{11}$$

we have

$$\begin{aligned}\Delta d_k(\mathbf{p}) &= d_k(\mathbf{p}) - d \\ &= d\left(\sqrt{1 + \frac{x_k^2}{d^2} - \frac{2x_k \sin\theta}{d}} - 1\right) \\ &= d\left(\sqrt{f_k(\theta, d)} - 1\right)\end{aligned} \tag{12}$$

where $f_k(\theta, d)$ represents the curvature information and it is defined as [51]

$$f_k(\theta, d) = 1 + \frac{x_k^2}{d^2} - \frac{2x_k \sin\theta}{d}. \tag{13}$$

[3]The CRLB indicates the lower bound on the variance for the estimation of a deterministic parameter, such as the phase in this case (i.e., the best estimation accuracy) [47].

[4]In the case of highly dynamic scenarios due to high-speed mobility, instead of considering averaging among M_p phase estimates, it could be convenient performing M_p successive position estimates.

Finally, we can gather all the differential phase information in the following observation vectors

$$\mathbf{\Phi} = \left[\mathbf{\Phi}_0, \mathbf{\Phi}_1, \dots, \mathbf{\Phi}_l, \dots, \mathbf{\Phi}_{N_\mathrm{p}-1}\right]^\top \in \mathbb{R}^{K_\mathrm{a} \times N_\mathrm{p}} \tag{14}$$

$$\mathbf{\Phi}_l = \left[\Delta\phi_{l,0}, \Delta\phi_{l,1}, \dots, \Delta\phi_{l,k}, \dots, \Delta\phi_{l,K_\mathrm{a}-1}\right]^\top \in \mathbb{R}^{K_\mathrm{a} \times 1}. \tag{15}$$

2) Derivation of the Lower Bound on the Position Estimation Accuracy: We now derive the CRLB on the relative localization accuracy, expressed in terms of bearing and ranging of the transmitting vehicle. Following the same steps as in [51], the CRLB on $\mathbf{p} = [\theta, d]^\top \in \mathbb{R}^2$, indicated with $\mathbf{\Sigma}(\mathbf{p})$, can be written as

$$\mathbf{\Sigma}(\mathbf{p}) \triangleq \mathbf{J}^{-1}(\mathbf{p}) = \left[\sum_{l=0}^{N_\mathrm{p}-1} \mathbf{J}_l(\mathbf{p})\right]^{-1} \tag{16}$$

where $\mathbf{J}$ and $\mathbf{J}_l$ are, respectively, the total Fisher information matrix (FIM) and the FIM related to the l-th frequency pilot. In (16) we have exploited the additive property of FIM, as in [52, Eq. 27]. The generic element of the FIM $\mathbf{J}_l$ is given by

$$[\mathbf{J}_l(\mathbf{p})]_{11} = J_l^{(\theta,\theta)}(\mathbf{p}) = \mathbb{E}_{\mathbf{\Phi}_l|\mathbf{p}}\left\{\left(\frac{\partial \ln p(\mathbf{\Phi}_l|\mathbf{p})}{\partial\theta}\right)^2\right\} \tag{17}$$

$$[\mathbf{J}_l(\mathbf{p})]_{22} = J_l^{(d,d)}(\mathbf{p}) = \mathbb{E}_{\mathbf{\Phi}_l|\mathbf{p}}\left\{\left(\frac{\partial \ln p(\mathbf{\Phi}_l|\mathbf{p})}{\partial d}\right)^2\right\} \tag{18}$$

$$[\mathbf{J}_l(\mathbf{p})]_{12} = J_l^{(\theta,d)}(\mathbf{p}) = \mathbb{E}_{\mathbf{\Phi}_l|\mathbf{p}}\left\{\frac{\partial \ln p(\mathbf{\Phi}_l|\mathbf{p})}{\partial\theta\partial\ d}\right\} \tag{19}$$

and $[\mathbf{J}_l(\mathbf{p})]_{21} = [\mathbf{J}_l(\mathbf{p})]_{12}$, where $\ln p(\mathbf{\Phi}_l|\mathbf{p})$ is the log-likelihood function of the observation $\mathbf{\Phi}_l$ according to the model in (9), that is[5]

$$\ln p(\mathbf{\Phi}_l|\mathbf{p}) \propto -\frac{1}{4\sigma_\phi^2}\sum_{k=0}^{K_\mathrm{a}-1}\left(\Delta\phi_{l,k} - \Delta\xi_{l,k}(\mathbf{p})\right)^2. \tag{20}$$

Consequently, by applying the expected value in (17)-(19), it is straightforward to obtain [53]

$$J_l^{(\theta,\theta)}(\mathbf{p}) = \frac{1}{2\sigma_\phi^2}\sum_{k=0}^{K_\mathrm{a}-1}\left(\frac{\partial\Delta\xi_{l,k}(\mathbf{p})}{\partial\theta}\right)^2 \tag{21}$$

$$J_l^{(d,d)}(\mathbf{p}) = \frac{1}{2\sigma_\phi^2}\sum_{k=0}^{K_\mathrm{a}-1}\left(\frac{\partial\Delta\xi_{l,k}(\mathbf{p})}{\partial d}\right)^2 \tag{22}$$

$$J_l^{(\theta,d)}(\mathbf{p}) = \frac{1}{2\sigma_\phi^2}\sum_{k=0}^{K_\mathrm{a}-1}\left(\frac{\partial\Delta\xi_{l,k}(\mathbf{p})}{\partial d\,\partial\theta}\right). \tag{23}$$

The derivatives above are given by, respectively,

$$\frac{\partial\Delta\xi_{l,k}(\mathbf{p})}{\partial\theta} = \frac{2\pi dx_k\cos\theta}{\lambda_l\sqrt{d^2 + x_k^2 - 2dx_k\sin\theta}} \tag{24}$$

$$\frac{\partial\Delta\xi_{l,k}(\mathbf{p})}{\partial d} = -\frac{2\pi\left(d - x_k\sin\theta - \sqrt{d^2 + x_k^2 - 2dx_k\sin\theta}\right)}{\lambda_l\sqrt{d^2 + x_k^2 - 2dx_k\sin\theta}} \tag{25}$$

$$\frac{\partial\Delta\xi_{l,k}(\mathbf{p})}{\partial\theta\partial d} = -\frac{2\pi x_k^2\cos\theta\,(d\sin\theta - x_k)}{\lambda_l\sqrt{(d^2 + x_k^2 - 2dx_k\sin\theta)^3}}. \tag{26}$$

[5]We omit the mod operator in order to meet the regularity conditions for the sake of CRLB derivation.

Then, the error bounds on bearing (i.e., AoA estimation) and ranging (i.e., distance estimation) are respectively given by

$$\mathsf{BEB} = \sqrt{[\mathbf{\Sigma}(\mathbf{p})]_{1,1}}, \quad \mathsf{REB} = \sqrt{[\mathbf{\Sigma}(\mathbf{p})]_{2,2}} \tag{27}$$

that express a lower bound on the accuracy of position $\mathbf{p}$ (expressed as components of polar coordinates) of the transmitting NV with respect to the receiving AV where the center of the reference system is placed. In order to derive the bound on the relative localization accuracy, thus merging the information coming from bearing and ranging estimates, we can write the position error bound (PEB) by considering the same method as in [54, Eq. 8-10], thus using the transformation from polar to Cartesian coordinates according to $\tilde{\mathbf{J}}(\tilde{\mathbf{p}}) = \mathbf{C}^{\top}(\mathbf{p})\,\mathbf{J}(\mathbf{p})\,\mathbf{C}(\mathbf{p})$ where $\mathbf{C}(\mathbf{p})$ is the Jacobian matrix defined as

$$\mathbf{C}(\mathbf{p}) = \begin{bmatrix} \frac{\partial\theta}{\partial x} & \frac{\partial\theta}{\partial y} \\ \frac{\partial d}{\partial x} & \frac{\partial d}{\partial y} \end{bmatrix} = \begin{bmatrix} -\frac{\sin(\theta)}{d} & \frac{\cos(\theta)}{d} \\ \cos(\theta) & \sin(\theta) \end{bmatrix}. \tag{28}$$

Hence we have

$$\begin{aligned}\left[\tilde{\mathbf{J}}(\tilde{\mathbf{p}})\right]_{11} &= J^{(x,x)}(\tilde{\mathbf{p}}) = \frac{\sin^2(\theta)}{d^2} J^{(\theta,\theta)}(\mathbf{p}) \\ &\quad + \cos^2(\theta) J^{(d,d)}(\mathbf{p}) - 2\cos(\theta)\frac{\sin(\theta)}{d} J^{(\theta,d)}(\mathbf{p})\end{aligned} \tag{29}$$

$$\begin{aligned}\left[\tilde{\mathbf{J}}(\tilde{\mathbf{p}})\right]_{22} &= J^{(y,y)}(\tilde{\mathbf{p}}) = \frac{\cos^2(\theta)}{d^2} J^{(\theta,\theta)}(\mathbf{p}) \\ &\quad + \sin^2(\theta) J^{(d,d)}(\mathbf{p}) + 2\frac{\cos(\theta)}{d}\sin(\theta) J^{(\theta,d)}(\mathbf{p})\end{aligned} \tag{30}$$

$$\begin{aligned}\left[\tilde{\mathbf{J}}(\tilde{\mathbf{p}})\right]_{12} &= J^{(x,y)}(\tilde{\mathbf{p}}) = -\frac{\sin(\theta)\cos(\theta)}{d^2} J^{(\theta,\theta)}(\mathbf{p}) \\ &\quad + \sin(\theta)\cos(\theta) J^{(d,d)}(\mathbf{p}) \\ &\quad + 2\sin(\theta)\frac{\cos(\theta)}{d} J^{(\theta,d)}(\mathbf{p})\end{aligned} \tag{31}$$

and $[\tilde{\mathbf{J}}(\tilde{\mathbf{p}})]_{21} = [\tilde{\mathbf{J}}(\tilde{\mathbf{p}})]_{12}$. Then, the PEB is given by

$$\mathsf{PEB} = \sqrt{\mathrm{tr}\left(\tilde{\mathbf{J}}^{-1}(\tilde{\mathbf{p}})\right)} \tag{32}$$

allowing to define the bound on the estimation for the relative position $\mathbf{p}$ of the transmitting NV with respect to the receiving AV equipped with the large ULA. When vehicles travel in the same direction (e.g., the platooning scenario in straight highway), the element $[\tilde{\mathbf{J}}^{-1}(\tilde{\mathbf{p}})]_{11}$ denotes the accuracy along the x axis, i.e., the *lateral accuracy*; differently, the element $[\tilde{\mathbf{J}}^{-1}(\tilde{\mathbf{p}})]_{22}$ denotes the accuracy along the y axis, i.e., the *longitudinal accuracy*, which is of primary interest for the correct management of the platoon at constant inter-vehicle distance [8].

a) Remarks on bearing information: By considering (17), (21) and (24) we obtain that the element $[\mathbf{J}(\mathbf{p})]_{11}$ referring to the bearing information is

$$J^{(\theta,\theta)}(\mathbf{p}) = \frac{4\pi^2 M_{\mathrm{p}} \mathsf{SNR}}{\eta} \sum_{l=0}^{N_{\mathrm{p}}-1} \sum_{k=0}^{K_{\mathrm{a}}-1} \frac{d^2 x_k^2 \cos^2\theta}{\lambda_l^2 (d^2 + x_k^2 - 2dx_k \sin\theta)}. \tag{33}$$

When the distance d becomes large with respect to the antenna size, the signal impinging on the ULA exhibits a planar wavefront. In this case, (33) returns

$$\begin{aligned}J^{(\theta,\theta)}(\mathbf{p}) &\approx \frac{4\pi^2 M_{\mathrm{p}} \mathsf{SNR}}{\eta} \sum_{l=0}^{N_{\mathrm{p}}-1} \sum_{k=0}^{K_{\mathrm{a}}-1} \frac{x_k^2 \cos^2\theta}{\lambda_l^2} \\ &= \frac{4\pi^2 M_{\mathrm{p}} \mathsf{SNR} \cos^2\theta}{\eta} \sum_{l=0}^{N_{\mathrm{p}}-1} \frac{2}{\lambda_l^2} \left(\frac{\lambda}{2}\right)^2 \sum_{k=0}^{\frac{K_{\mathrm{a}}-1}{2}} k^2 \\ &\approx \frac{\pi^2 M_{\mathrm{p}}\, N_{\mathrm{p}}\, \mathsf{SNR}\, K_{\mathrm{a}} (K_{\mathrm{a}}^2 - 1)\cos^2\theta}{12\,\eta}\end{aligned} \tag{34}$$

where in the last approximation we considered $\lambda_l \approx \lambda\, \forall l$. Equation (34) results in the inverse of the traditional CRLB for bearing estimation using a (small) $\lambda/2$-spaced ULA, thus under the approximation of planar wavefront propagation. In this case, the AoA estimation accuracy is maximum for $\theta = 0$ (boresight direction), while AoA estimation is not possible for $\theta = \pm\pi/2$.

b) Remarks on ranging information: Following the same steps as before and considering (18), (22), and (25) for ranging information, we obtain that the element $[\mathbf{J}(\mathbf{p})]_{22} = J^{(d,d)}(\mathbf{p})$ is

$$\begin{aligned}J^{(d,d)}(\mathbf{p}) &= \frac{4\pi^2 M_{\mathrm{p}} \mathsf{SNR}}{\eta} \\ &\quad \times \sum_{l=0}^{N_{\mathrm{p}}-1} \sum_{k=0}^{K_{\mathrm{a}}-1} \frac{1}{\lambda_l^2 (d^2 + x_k^2 - 2dx_k \sin\theta)} \\ &\quad \times \Big[2d^2 + x_k^2(1 + \sin^2\theta) - 4dx_k \sin\theta \\ &\quad - 2(d - x_k \sin\theta)\sqrt{d^2 + x_k^2 - 2dx_k \sin\theta}\Big].\end{aligned} \tag{35}$$

From (35) it can be noticed that $J^{(d,d)}(\mathbf{p}) \to 0$ for $d \to \infty$. In fact, at a large distance from a ULA, no information concerning the range can be obtained (case of planar wavefront propagation).

Some particular cases can be analyzed. At the boresight direction (i.e., for $\theta = 0$), the Fisher information concerning the ranging accuracy is given by

$$\begin{aligned}&J^{(d,d)}(\theta = 0, d) \\ &= \frac{4\pi^2 M_{\mathrm{p}} \mathsf{SNR}}{\eta} \sum_{l=0}^{N_{\mathrm{p}}-1} \sum_{k=0}^{K_{\mathrm{a}}-1} \frac{2d^2 + x_k^2 - 2d\sqrt{d^2 + x_k^2}}{\lambda_l^2 \sqrt{d^2 + x_k^2}}.\end{aligned} \tag{36}$$

Differently, for $\theta = \pm\pi/2$, where AoA estimation cannot be realized, we have

$$\begin{aligned}&J^{(d,d)}\left(\theta = \pm\frac{\pi}{2}, d\right) = \frac{4\pi^2 M_{\mathrm{p}} \mathsf{SNR}}{\eta} \\ &\quad \times \sum_{l=0}^{N_{\mathrm{p}}-1} \sum_{k=0}^{K_{\mathrm{a}}-1} \frac{1}{\lambda_l^2 (d - x_k)^2} \left[2(d - x_k)^2 - 2(d - x_k)^2\right] \\ &\quad = 0.\end{aligned} \tag{37}$$

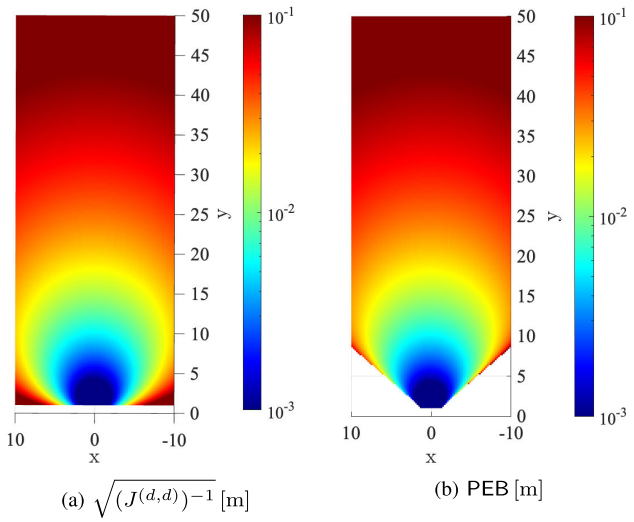

(a) $\sqrt{(J^{(d,d)})^{-1}}$ [m] (b) PEB [m]

Fig. 2. Error distribution in the half-space ahead a ULA placed at $(x, y) = (0, 0)$ with $D = 1\,\mathrm{m}$ and $f_\mathrm{c} = 5.9\,\mathrm{GHz}$, for $\mathsf{SNR} = 20\,\mathrm{dB}$.

Thus, neither angle nor distance can be estimated in the direction along which the array is deployed (blind direction).

c) Numerical example: As example, Fig. 2 reports the error distribution in the half-space ahead a receiving ULA, supposed on-board an AV deployed along the x axis and placed at $(x, y) = (0, 0)$ of maximum size $D = 1\,\mathrm{m}$, assuming $f_\mathrm{c} = 5.9\,\mathrm{GHz}$ and $\mathsf{SNR} = 20\,\mathrm{dB}$. On the left (Fig. 2a), the inverse of the ranging information $J^{(d,d)}(\mathbf{p})$ is reported (in square root). It is possible to notice that the area close to the array (in particular on its boresight direction, i.e., along the y axis from the array center at $x = 0$) is where the distance information can be obtained more reliably. Thus, range information is particularly accurate when the vehicles are aligned and at close distance, as happens when considering platooning in highway scenarios, where road curves are particularly smooth. Differently, when the distance d becomes large or the angle θ approaches $\pi/2$, the ranging accuracy severely degrades. The distribution of the PEB in the same area (thus the maximum localization accuracy of a transmitting NV) is reported on the right (Fig. 2b), thus including the effect of both ranging and bearing. It is possible to notice that the PEB follows the behavior of the Fig. 2a; thanks to the adoption of a very large array, AoA estimation is performed with high accuracy and, with good approximation, we have $\mathsf{PEB} \approx \mathsf{REB} \approx \sqrt{(J^{(d,d)})^{-1}}$. However, localization cannot be always realized since both ranging and bearing estimates become unreliable when the angle θ increases at a close distance from the antenna for angles larger than $\pi/4$. Different array geometries could be considered to counteract this phenomenon, e.g., circular or conformal arrays on the vehicle. Positioning is thus possible when the NV and the AV are close to each other so that near-field conditions are easily satisfied. In fact, in this region, the phase along the receiving array is highly non-linear, thus enabling the extraction of the distance information. As the distance increases, the planar wavefront approximation on the receiving array becomes gradually satisfied, resulting in a linear phase profile from which bearing only can be inferred.

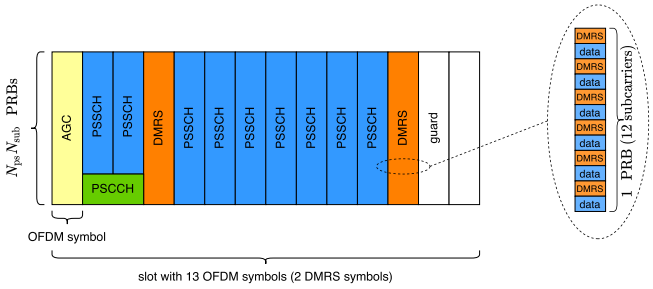

Fig. 3. Example of a slot with 13 OFDM symbols. Time pattern relative to $M_\mathrm{p} = 2$ OFDM symbols reserved to DMRS per slot.

IV. Case Study: Implementation Using 5G NR-V2X Sidelink

In this section, we discuss how near-field localization of vehicles could be implemented when considering the features of 5G NR-V2X sidelink communications in relationship with its PHY layer, channels, reference signals, and resource allocation policies.

A. 5G NR-V2X PHY

At the PHY layer, the 5G NR-V2X radio resources (RRs) cover time and frequency domain. The resource element (RE) indicates a subcarrier over one OFDM symbol. The elementary time domain entity is given by the slot, composed of 14 OFDM symbols, when the standard cyclic prefix is adopted, as assumed in this work; then, a subframe can be composed of one or more slots. Organization of RRs in the frequency domain encompasses subchannels and physical resource blocks (PRBs); a subchannel consists of N_ps consecutive PRBs, where N_ps can be selected among the values in the set $\{10, 12, 15, 20, 25, 50, 75, 100\}$. A PRB comprises 12 consecutive subcarriers with SCS given by Δf. Then, the single PRB exhibits a variable bandwidth depending on the selected SCS. The smallest allocation unit in the frequency domain is one subchannel (i.e., N_ps consecutive PRBs) so that a packet transmission spans one slot in the time domain and N_sub contiguous subchannels in the frequency domain, depending on the size of the packet to transmit. Thus, one sidelink data transmission occupies $M = 14$ OFDM symbols and $N = 12 N_\mathrm{ps} N_\mathrm{sub}$ subcarriers (see Fig. 3).

For the FR1 band, the allowed SCS values are $\Delta f = \{15, 30, 60\}\,\mathrm{kHz}$, corresponding to slot duration of $\{1, 0.5, 0.25\}\,\mathrm{ms}$, respectively. With the increasing of the SCS the slot duration decreases, and the number of slots per subframe increases; on the other side, the bandwidth of a PRB increases, thus the number of available resources at a given radio channel decreases, requiring adopting higher modulation and coding schemes (MCSs) to accommodate the data.

B. 5G NR-V2X Channels

For sidelink communication, NR defines four sidelink physical channels, *(i)* the Physical sidelink shared channel (PSSCH), *(ii)* the Physical sidelink control channel (PSCCH), *(iii)* the Physical sidelink feedback channel (PSFCH), and *(iv)* the Physical sidelink broadcast channel (PSBCH) each characterized by a specific set of resource elements. The sidelink physical channel carrying data transmitted by the vehicle is the PSSCH, thus occupying most of the RRs. For this

reason, in this work, we consider the use of PSSCH for localization of NVs. The PSSCH also contains synchronization and control information and a part of the sidelink control information (SCI). Several modulation formats can be adopted for PSSCH, enabling to adjust the spectral efficiency and the throughput, at the expense of sidelink coverage, depending on the application requirements.

PSSCH can be transmitted starting from the second OFDM symbol in a slot, and it can occupy 5 to 12 consecutive OFDM symbols. In order to realize near-field localization, pilot transmissions are required to collect the phase observations (7). Among the different reference signals foreseen in NR, such as synchronization and phase tracking reference signals, we consider here the exploitation of the demodulation reference signal (DMRS), which is sent together with the PSSCH and that is discussed in the following paragraph.

C. Pilot Scheme and Resource Occupation

The DMRS is a sidelink physical signal that does not carry information originating from the UE, and it is used for channel state information estimation and, thus, data demodulation. In particular, DMRS is associated with the corresponding physical channel (e.g., PSSCH) and multiplexed in time and frequency between the UE data. The transmission of the pilot symbols corresponding to DMRS is realized at configurable positions inside the slot and at configurable density in the time domain, thus allowing coping with different vehicular speeds (e.g., the time density of DMRS is larger in high-speed scenarios where fast changes of the radio channel are expected).[6] Specifically, nine distinct patterns in the time domain are supported for DMRS pilots, and the number of slots containing such pilots can span from 2 to 4, so that $M_{\mathrm{p}} = \{2, 3, 4\}$. Then, in the frequency domain, DMRS pilots follow the type 1 pattern configuration [29], which corresponds to alternating subcarriers with UE data, and a total of 6 pilots over 12 subcarriers per PRB (see Fig. 3). Thus, depending on the number of subchannels N_{sub} and the number of PRBs per subchannel N_{ps}, the number of frequency pilots per sidelink data transmission is $N_{\mathrm{p}} = N/2 = 6N_{\mathrm{ps}}N_{\mathrm{sub}}$. Of course, the packet size impacts the number of required subchannels and, consequently, the number of DMRS to be used for localization, thus its accuracy.

It can be noticed how, among the $12 \times 14 = 168$ REs in a slot and for a single PRB, DMRS can occupy 12, 18, 24 of these REs, corresponding to $M_{\mathrm{p}} = 2, 3, 4$, respectively.[7] Then, the other REs can be exploited for data; depending on the selected MCS, the minimum amount of PRBs $N^{\star}_{\mathrm{PRB}}$ required to accommodate a packet of a given size is reported in Tab. I. When a high number of DMRS is used (i.e., $M_{\mathrm{p}} = 4$), the number of PRBs needed to accommodate data increases, especially for low MCS.

D. Resource Allocation

RRs must be dynamically assigned to the transmitting vehicles in the scenario to minimize collisions and interference [9], [29], [55]. In 5G NR-V2X, two resource allocation policies are considered, named *Mode 1* and *Mode 2*. In *Mode 1*, the presence of the cellular network is mandatory (controlled mode); *Mode 2*, differently, can also operate in out-of-coverage conditions. According to this mode, the vehicle autonomously selects the sidelink radio resources by exploiting a channel sensing mechanism based on analyzing the received power at a given RR. Since *Mode 2* can operate without network coverage, it is considered the baseline for safety applications that cannot depend on the availability of cellular coverage. Thus, this resource allocation mode is also of interest when considering the positioning of vehicles using V2X sidelink, which must work independently of the network availability. When operating with the autonomous mode, it is likely that the same pool of resources can be shared (also in part) among different vehicles due to the distributed allocation mechanism. This fact produces interference that impacts communication and localization performance, as it will be discussed with the numerical results of Sec. V.

TABLE I
NUMBER OF PRBS NEEDED TO ACCOMMODATE A DATA PACKET OF A GIVEN SIZE, FOR DIFFERENT NUMBERS M_{p} OF OFDM SYMBOLS RESERVED TO DRMS

MCS	$N^{\star}_{\mathrm{PRB}}$ (350 bytes)			$N^{\star}_{\mathrm{PRB}}$ (1000 bytes)		
	$M_{\mathrm{p}}=2$	$M_{\mathrm{p}}=3$	$M_{\mathrm{p}}=4$	$M_{\mathrm{p}}=2$	$M_{\mathrm{p}}=3$	$M_{\mathrm{p}}=4$
0	97	101	107	265	278	292
1	75	78	82	203	213	224
2	61	64	68	166	174	183
3	48	50	53	128	135	141
4	40	42	44	105	110	116
5	33	34	36	86	90	95
6	28	30	31	73	77	81
7	25	26	27	63	66	69
8	22	23	24	55	58	61
9	20	21	22	50	52	54
10	20	21	22	49	52	54
11	18	19	20	45	47	49
12	16	17	18	39	41	43
13	15	15	16	35	37	39
14	13	14	15	32	33	35
15	12	13	14	29	30	32
16	12	12	13	27	28	30
17	12	12	13	27	28	30
18	11	12	12	26	27	28
19	10	11	11	23	25	26
20	10	10	11	22	23	24
21	9	10	10	20	21	22
22	9	9	10	19	20	21
23	8	9	9	18	19	20
24	8	8	9	17	18	18
25	8	8	9	16	17	18
26	8	8	8	15	16	17
27	7	8	8	15	15	16
28	7	7	8	14	15	16

V. NUMERICAL RESULTS

A. Simulation Environment

The performance of 5G NR-V2X sidelink localization in realistic operating environments is characterized through the exploitation of a system-level simulator, realized starting from the open-source simulator WiLabV2Xsim [56]. WiLabV2Xsim is an event-driven simulator, originally designed

[6]The different time patterns for the PSSCH DMRS depend on the number of symbols for PSCCH, the number of symbols including DMRS, and the number of symbols for PSSCH within a slot [29]. The selected set of positions of DMRS in the slot is indicated in the SCI.

[7]Other configurations are possible. See [29] for details.

to characterize resource allocation techniques for V2X connectivity. It considers the flexible numerology and PHY layer aspects together with the sidelink resource allocation policies for 5G NR-V2X communications, including generation of the messages (here considered periodic) and a typical medium access control (MAC) layer implementation. Specifically, the simulator reproduces a scenario with multiple vehicles moving and transmitting packets using the 5G NR-V2X sidelink interface. The 5G protocol stack is implemented for each transmitted packet, including autonomous resource allocation policies according to *Mode 2*, and, for each packet, the signal-to-interference-plus-noise ratio (SINR) related to packets received by the nearby vehicles is evaluated. In this manner, the characterization of the performance can include all the relevant system-level parameters such as MCS, SCS, transmitted power, packet size and generation statistics, and channel bandwidth, as well as the scenario-related parameters, such as density of vehicles, speed, etc. Considering the time instant $t \in \mathcal{T}$, where $\mathcal{T}$ is the set of time instants of the simulation, the set of vehicles having packets to transmit is indicated with $\mathcal{I}_t$. Then, the SINR related to the reception of the i-th packet, with $i \in \mathcal{I}_t$, by the j-th vehicle is given by

$$\mathsf{SINR}_{t,ij} = \frac{P_{\mathrm{R}ij}}{P_{\mathrm{n}} + I_{t,j}} \tag{38}$$

where $P_{\mathrm{R}ij}$ is the received power at vehicle j from vehicle i, $P_{\mathrm{n}} = N\sigma^2$ is the noise power. The interference at the receiving vehicle j coming from other vehicles transmitting at the same time slot t is accounted by the term $I_{t,j}$ and is given by

$$I_{t,j} = \sum_{k \in \mathcal{I}_t, k \neq i} \eta_{t,kj} \frac{P_{\mathrm{T}}\, g_{t,kj}}{L(d_{t,kj})} \tag{39}$$

where the term $L(d_{t,kj})$ is the path loss at a distance $d_{t,kj}$ between the interfering transmitting vehicle k and the receiving vehicle j at t, $g_{t,kj}$ is the large-scale fading contribution related to the link between the interfering transmitting vehicle k and the receiving vehicle j at t, and $\eta_{t,kj}$ is a coefficient between 0 and 1 accounting for the partial overlap between the resources allocated for the transmission of the vehicle i and those allocated for the transmission of the vehicle k (i.e., interference). Note that the interference level and, consequently, the localization performance are affected by the distribution of vehicles in the scenario, the resource allocation mechanism, the packet size, and the packet generation statistic.

The main settings adopted for the simulations are reported in Tab. II and discussed hereafter. We consider a highway scenario with three lanes per direction and a variable number of vehicles per kilometer (variable vehicle density). Each vehicle moves with an average speed of $70\,\mathrm{km/h}$ and a standard deviation of $7\,\mathrm{km/h}$. Simulation parameters are taken from the standard evaluation scenario indicated in [29, Tab. XII]. The channel between vehicles, for what concerns path loss characterization determining the interference level in (39), is modeled according to the WINNER+, scenario B1, with correlated log-normally distributed shadowing, characterized by a standard deviation of $3\,\mathrm{dB}$ and a decorrelation distance of $25\,\mathrm{m}$, as suggested in [57].

TABLE II
SIMULATION PARAMETERS

Parameter	Symbol	Value
Transmitted power	P_{T}	$23\,\mathrm{dBm}$
Antenna gain	G	$3\,\mathrm{dB}$
Frequency	f_{c}	$5.9\,\mathrm{GHz}$
Receiver noise figure	F	$9\,\mathrm{dB}$
Available channel bandwidth	W_{ch}	$10\,\mathrm{MHz}$
SCS	Δf	15 kHz
MCS	--	5, 15, 23
Packet size	--	350, 1000 bytes
Packet generation interval	T_{g}	$100\,\mathrm{ms}$
# of ODFM symbols	M	14
Implementation loss	η	$6\,\mathrm{dB}$
Average vehicle speed	--	$70\,\mathrm{km/h}$
STD of vehicle speed	--	$7\,\mathrm{km/h}$
Vehicle density (veh./km)	--	50, 100, 150, 200

B. Localization Performance in Vehicular Scenarios

The proposed localization approach is here characterized according to the following performance metrics:

1) The average PEB for the vehicles located at a certain distance from the receiving AV, evaluated according to (32). For each transmitting vehicle (i.e., NV), the relative distance and orientation with respect to the set of receivers are evaluated with the simulator, together with the corresponding SINR, allowing to build a set of PEB values. The PEB values are then averaged over the number of discrete time instants and vehicles, considering a certain distance.
2) The localization availability ratio (LAR), that indicates the rate of localization occurrences at a distance d presenting a PEB smaller than γd, where $\gamma < 1$ is a selected relative accuracy level.

These performance metrics, in addition to the localization update rate (LUR), which reports the number of positions estimated per second, allow to provide immediate insights in relationship with the first three KPIs listed in Sec. II-B as fundamentals for localization in vehicular contexts (i.e., accuracy, availability, update rate). The simulation results cannot directly infer latency; however, since the proposed scheme enables the direct localization of the transmitting vehicle, such latency is strictly related to the hardware and signal-processing implementations, thus guaranteeing the lowest one with respect to other schemes based on external anchors and/or cooperation among different mobile/fixed nodes.

1) Localization Accuracy: Figure 4a reports the average components of the PEB denoting the longitudinal and lateral accuracy as a function of the distance between transmitter and receiver, considering a ULA of $D \approx 1.2\,\mathrm{m}$ and $\delta = \lambda/2$ (corresponding to $K_{\mathrm{a}} = 41$ antennas) for different values of the vehicle density in the scenario. Packets of 350 bytes with MCS 15 are considered. The longitudinal PEB spans from the millimeter range at $d = 10\,\mathrm{m}$ up to the meter range at $d = 100\,\mathrm{m}$, increasing as the distance increases due to the larger errors in ranging estimates when the nonlinearity of the phase profile at the receiving antenna - characteristic of the near-field region and enabling ranging estimation - becomes less pronounced. It is possible to see the effect of the vehicle density, decreasing the average localization accuracy as the number of UEs in the scenario increases due to the higher interference level. When moving from 20 to 200 vehicles per

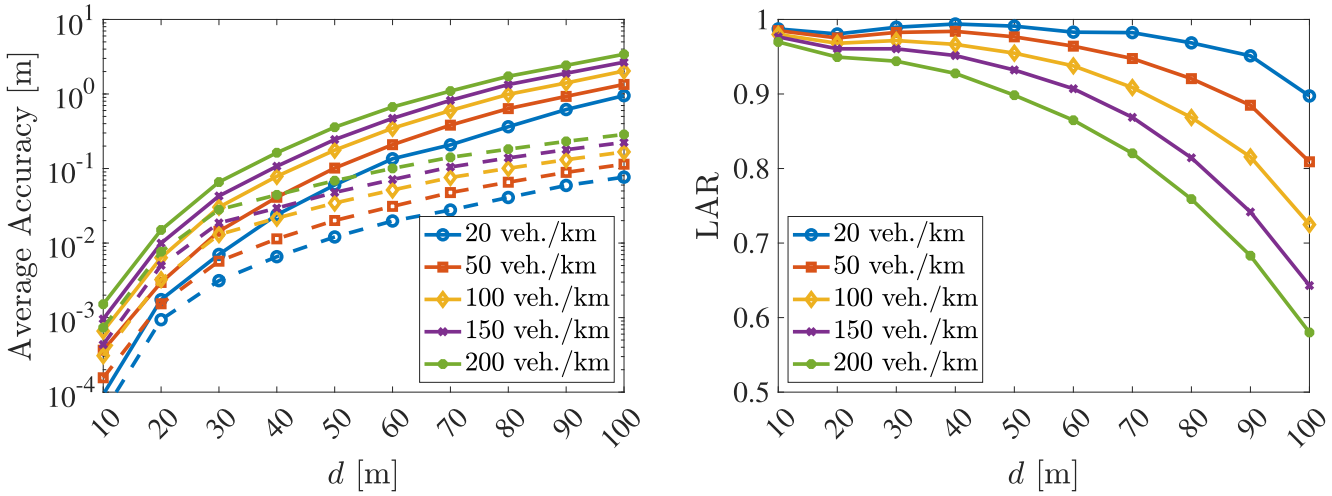

(a) (–) Longitudinal accuracy; (- -) Lateral accuracy

(b) Localization availability ratio

Fig. 4. Average localization accuracy (PEB) and localization availability ratio (LAR) as a function of the distance d for different densities of vehicles in the scenario. Packets of 350 bytes with MCS 15 are considered.

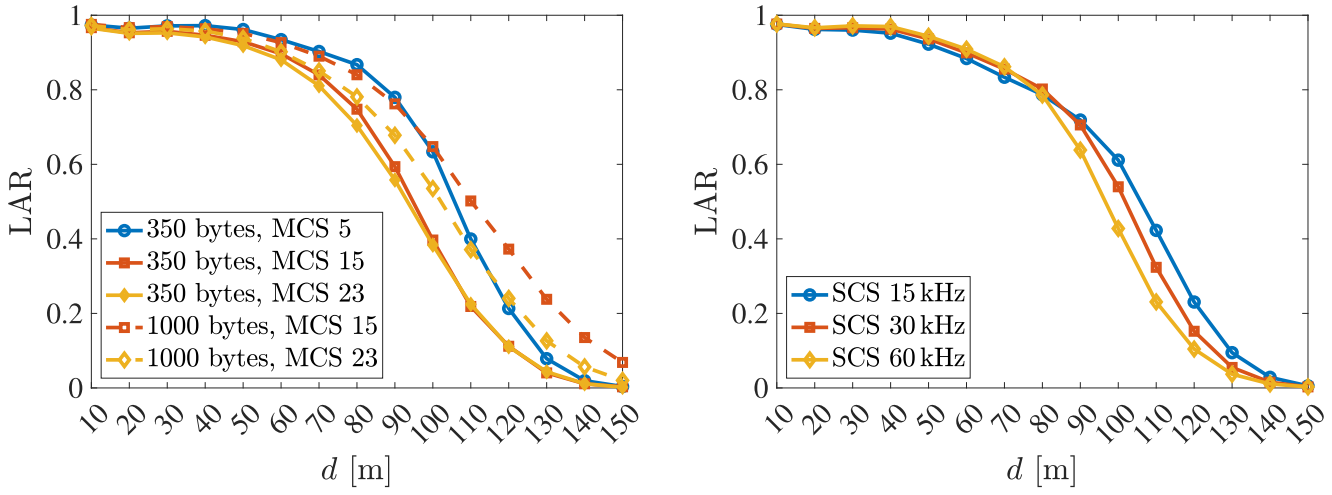

(a) Impact of packet size and MCS

(b) Impact of SCS

Fig. 5. Localization availability ratio (LAR) as a function of the distance d for different packet size, MCS and SCS.

kilometer of density, the average PEB can change even by one order of magnitude, thus showing how interference can severely impact performance in realistic conditions. It is interesting to notice that the longitudinal accuracy performance decreases faster with the distance. In fact, lateral accuracy is strongly impacted by the bearing estimate in the highway scenario considered, which is highly accurate thanks to the large array assumed.

2) Localization Availability: The LAR for the same setting is reported in Fig. 4b considering a threshold $\gamma = 0.01$, thus assuming a target accuracy of $1\,\mathrm{cm}$ at $d = 1\,\mathrm{m}$, or $1\,\mathrm{m}$ at $d = 100\,\mathrm{m}$. In this case, at a small distance, more than the 95% of the occurrences satisfy the very stringent accuracy target. Again, it is possible to notice that the interference due to multiple vehicles in the scenario should not be neglected, especially when the inter-vehicle distance grows large.

3) Impact of System-Level Parameters: The impact of MCS on the localization accuracy is reported in Fig. 5a. In particular, the LAR as a function of the distance d is presented for two packet sizes (350 and 1000 bytes) and for MCS 5, 15, and 23. For both packet sizes, if the MCS increases, the localization accuracy decreases. An increase of the MCS allows to transmit a packet with less PRBs according to Tab. I; thus, the smaller bandwidth occupied by a packet translates into a lower number of pilots N_{p} used for localization, and consequently poorer performance. For the same reason, fixing the MCS, a larger packet improves the performance. Of course, results could also change depending on the interference level since larger packets occupy more resources. Note that 1000 bytes with MCS 5 is not considered since such a configuration would not fit the $10\,\mathrm{MHz}$ channel bandwidth available. The impact of the SCS is shown in Fig. 5b. In this case, large SCS is beneficial at a low distance thanks to the higher robustness against interference (shorter packets in the time domain, thus lower probability of collision). Differently, when the distance grows, the larger SCS is not beneficial due to the larger amount of noise (larger bandwidth, thus lower SNR). However, the impact is visible only for large distances, where localization errors are intrinsically large.

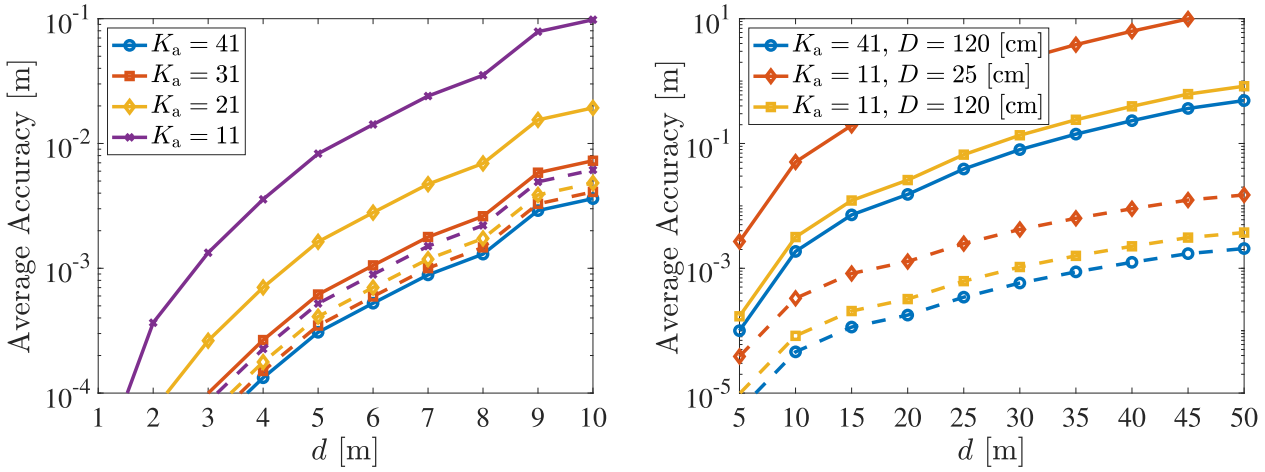

(a) (–) Fixed K_a, $\delta = \lambda/2$; (- -) Fixed D, variable δ

(b) (–) Longitudinal accuracy; (- -) Lateral accuracy

Fig. 6. Average localization accuracy (PEB) as a function of the distance d in platooning for different configurations of the receiving ULA.

In the considered scenario, a maximum LUR of 10 position updates per second per transmitting vehicle can be obtained since a packet generation interval $T_g = 100\,\text{ms}$ was considered (see Tab. II). In practical conditions, the rate will decrease at a larger distance due to the probability of packet loss caused by the larger path loss and susceptibility to interference. It is worth noting that by decreasing the packet generation interval T_g, the LUR increases accordingly. However, interference may play a crucial role due to the higher probability of collision (lower availability of radio resources to accommodate the different users).

C. Localization Performance in Platooning

Differently from the previous results that refer to a general highway scenario, Fig. 6 focuses on platooning. Thus, we consider only transmitting NV vehicles on the same lane of the receiving AV. Specifically, Fig. 6a shows the average PEB considering reduced distances between $1\,\text{m}$ and $10\,\text{m}$, typical for the platooning application. In all previous cases, a large array was considered to enable localization even at large distances. Here, the continuous lines assume a fixed number of antennas K_a at $\delta = \lambda/2$ spacing, thus different array sizes, from $D \approx 120\,\text{cm}$ (corresponding to $K_a = 41$) to $D \approx 25\,\text{cm}$ (corresponding to $K_a = 11$). As evident, the localization accuracy is severely impacted by decreasing the number of antennas (and thus, the array size). For example, at $d = 10\,\text{m}$, more than one order of magnitude of error difference is experienced when moving from $K_a = 41$ to $K_a = 11$. Differently, dashed lines consider the same number of antennas as before, spanning from $K_a = 41$ to $K_a = 11$, but fixing the array size to the largest value $D = 120\,\text{cm}$ (thus, with $\delta > \lambda/2$). It is interesting to notice that, in this case, even a reduced number of antennas enables a small performance reduction w.r.t. the best case. Localization resolution in the near field is mainly due to the array size (i.e., whole antenna aperture) rather than the number of antenna elements. This paves the way for significantly reducing the implementation complexity with small performance degradation. Finally, Fig. 6b shows the bound on the longitudinal and lateral localization accuracy for the platooning scenario in three different configurations: *(i)* large array with $\delta = \lambda/2$ spacing ($K_a = 41$), *(ii)* smaller array with $\lambda/2$ spacing ($K_a = 11$), and *(iii)* large array with $\delta > \lambda/2$ spacing ($K_a = 11$). As it is possible to notice, the longitudinal accuracy is mostly impacted by the array size since it is strictly related to the ranging information, which is more reliable when near-field conditions are easily satisfied. Also, in this case, a reduced number of antennas with large array size results in a small performance reduction with respect to large and dense arrays.

D. Concluding Remarks, Implementation Challenges, and Future Developments

The proposed results showed the potential of near-field localization in the V2X context, especially in scenarios with reduced inter-vehicle distance, such as platooning. From the implementation point of view, some challenges must be tackled in order to provide practical implementations. First, low-complexity algorithms need to be defined to gather the positioning information (i.e., range and angle) from the large antenna array by considering the near-field signal characteristics. Second, the realization of the large array must provide phase coherence along all the antenna elements in order to perform differential phase measurements as indicated in Sec. III. In this sense, the possibility of diminishing the number of antenna elements by enlarging the antenna spacing has been demonstrated as a viable solution to keep complexity low by preserving the near-field behavior. It is interesting to highlight that the future use of FR2 will make near-field conditions easier to obtain, according to (1), thus making position estimation feasible with smaller arrays and/or larger operating distances. Moreover, since mmWave operations usually require antenna arrays also at the transmitting side, this would pave the way to joint position and orientation estimation, i.e., computation of the heading of the transmitting vehicle, which is important as well for autonomous driving operations [8].

VI. Conclusion

In this paper, we proposed the use of V2X sidelink communication signals for positioning by considering the features of near-field propagation through the adoption of large antenna arrays and/or high-frequency to jointly estimate the ranging and bearing of a nearby vehicle (i.e., relative localization) without requiring any off-board positioning infrastructure or synchronization between vehicles. To this end, we derived

the performance limits of near-field V2X sidelink positioning. Through a 5G NR-V2X sidelink case study, we showed that high-accuracy, low-latency, and high update-rate positioning are achievable, provided that large arrays are adopted onboard vehicles. The proposed approach is particularly suitable for advanced applications like platooning; in this context, the reduced inter-vehicle distance makes near-field conditions easy to obtain even with relatively small arrays, thus providing the capability of high longitudinal accuracy (sub-cm ranging) needed to maintain a constant distance and react quickly in the case this one changes for any reason. In perspective, this will enable the real-time control of CAVs for automated and cooperative driving applications.

ACKNOWLEDGMENT

The authors thank Vittorio Todisco, Alessandro Bazzi, Stefania Bartoletti, Alberto Zanella, and Davide Dardari for fruitful discussions and their support with WiLabV2Xsim.

REFERENCES

[1] C. De Lima et al., "Convergent communication, sensing and localization in 6G systems: An overview of technologies, opportunities and challenges," *IEEE Access*, vol. 9, pp. 26902–26925, 2021.

[2] H. Chen, H. Sarieddeen, T. Ballal, H. Wymeersch, M.-S. Alouini, and T. Y. Al-Naffouri, "A tutorial on terahertz-band localization for 6G communication systems," *IEEE Commun. Surveys Tuts.*, vol. 24, no. 3, pp. 1780–1815, 3rd Quart., 2022.

[3] S. Bartoletti et al., "Positioning and sensing for vehicular safety applications in 5G and beyond," *IEEE Commun. Mag.*, vol. 59, no. 11, pp. 15–21, Nov. 2021.

[4] H. Wymeersch, G. Seco-Granados, G. Destino, D. Dardari, and F. Tufvesson, "5G mmWave positioning for vehicular networks," *IEEE Wireless Commun.*, vol. 24, no. 6, pp. 80–86, Dec. 2017.

[5] J. He, K. Yang, and H.-H. Chen, "6G cellular networks and connected autonomous vehicles," *IEEE Netw.*, vol. 35, no. 4, pp. 255–261, Jul. 2021.

[6] S. Bartoletti, N. Decarli, and B. M. Masini, "Sidelink 5G-V2X for integrated sensing and communication: The impact of resource allocation," in *Proc. IEEE Int. Conf. Commun. Workshops (ICC Workshops)*, Seoul, South Korea, May 2022, pp. 79–84.

[7] L. Pucci, E. Paolini, and A. Giorgetti, "System-level analysis of joint sensing and communication based on 5G new radio," *IEEE J. Sel. Areas Commun.*, vol. 40, no. 7, pp. 2043–2055, Jul. 2022.

[8] T. G. R. Reid et al., "Localization requirements for autonomous vehicles," *SAE Int. J. Connected Automated Vehicles*, vol. 2, no. 3, pp. 1–18, Sep. 2019.

[9] A. Bazzi, A. O. Berthet, C. Campolo, B. M. Masini, A. Molinaro, and A. Zanella, "On the design of sidelink for cellular V2X: A literature review and outlook for future," *IEEE Access*, vol. 9, pp. 97953–97980, 2021.

[10] "System architecture and solution development; high-accuracy positioning for C-V2X," 5GAA Automot. Assoc., Munich, Germany, Tech. Rep., 2021. [Online]. Available: https://5gaa.org/content/uploads/2021/02/5GAA_A-200118_TR_V2XHAP.pdf

[11] *Study on Positioning Use Cases*, document TS 36.213, V16.2.0, 3GPP, Mar. 2018.

[12] S.-W. Ko, H. Chae, K. Han, S. Lee, D.-W. Seo, and K. Huang, "V2X-based vehicular positioning: Opportunities, challenges, and future directions," *IEEE Wireless Commun.*, vol. 28, no. 2, pp. 144–151, Apr. 2021.

[13] G. M. Hoangt, B. Denis, J. Härri, and D. Slock, "Cooperative localization in VANETs: An experimental proof-of-concept combining GPS, IR-UWB ranging and V2V communications," in *Proc. 15th Workshop Positioning, Navigat. Commun. (WPNC)*, Oct. 2018, pp. 1–6.

[14] J.-H. Ahn and J.-H. Won, "Localization based on lidar and GNSS for connected vehicles," in *Proc. IEEE/ION Position, Location Navigat. Symp. (PLANS)*, Apr. 2020, pp. 908–914.

[15] B. Soner and S. Coleri, "Visible light communication based vehicle localization for collision avoidance and platooning," *IEEE Trans. Veh. Technol.*, vol. 70, no. 3, pp. 2167–2180, Mar. 2021.

[16] B. W. Kim and S.-Y. Jung, "Vehicle positioning scheme using V2V and V2I visible light communications," in *Proc. IEEE 83rd Veh. Technol. Conf. (VTC Spring)*, May 2016, pp. 1–5.

[17] Q. Liu et al., "A highly accurate positioning solution for C-V2X systems," *Sensors*, vol. 21, no. 4, p. 1175, Feb. 2021. [Online]. Available: https://www.mdpi.com/1424-8220/21/4/1175

[18] S. Ma, F. Wen, X. Zhao, Z.-M. Wang, and D. Yang, "An efficient V2X based vehicle localization using single RSU and single receiver," *IEEE Access*, vol. 7, pp. 46114–46121, 2019.

[19] A. Ghods, S. Severi, and G. Abreu, "Localization in V2X communication networks," in *Proc. IEEE Intell. Vehicles Symp. (IV)*, Jun. 2016, pp. 5–9.

[20] J. Lota, S. Ju, O. Kanhere, T. S. Rappaport, and A. Demosthenous, "MmWave V2V localization in MU-MIMO hybrid beamforming," *IEEE Open J. Veh. Technol.*, vol. 3, pp. 210–220, Apr. 2022.

[21] W. Meng, X. Chu, Z. Lu, L. Wang, X. Wen, and M. Li, "V2V communication assisted cooperative localization for connected vehicles," in *Proc. IEEE Wireless Commun. Netw. Conf. (WCNC)*, Mar. 2021, pp. 1–6.

[22] H. Bagheri et al., "5G NR-V2X: Toward connected and cooperative autonomous driving," *IEEE Commun. Standards Mag.*, vol. 5, no. 1, pp. 48–54, Mar. 2021.

[23] F. Guidi and D. Dardari, "Radio positioning with EM processing of the spherical wavefront," *IEEE Trans. Wireless Commun.*, vol. 20, no. 6, pp. 3571–3586, Jun. 2021.

[24] Z. Abu-Shaban, K. Keykhosravi, M. F. Keskin, G. C. Alexandropoulos, G. Seco-Granados, and H. Wymeersch, "Near-field localization with a reconfigurable intelligent surface acting as lens," in *Proc. IEEE Int. Conf. Commun. (ICC)*, Jun. 2021, pp. 1–6.

[25] A. Elzanaty, A. Guerra, F. Guidi, D. Dardari, and M.-S. Alouini, "Toward 6G holographic localization: Enabling technologies and perspectives," *IEEE Internet Things Mag.*, vol. 6, no. 3, pp. 138–143, Sep. 2023.

[26] A. A. D'Amico, A. D. J. Torres, L. Sanguinetti, and M. Win, "Cramér–Rao bounds for holographic positioning," *IEEE Trans. Signal Process.*, vol. 70, pp. 5518–5532, 2022.

[27] K. Ganesan, J. Lohr, P. B. Mallick, A. Kunz, and R. Kuchibhotla, "NR sidelink design overview for advanced V2X service," *IEEE Internet Things Mag.*, vol. 3, no. 1, pp. 26–30, Mar. 2020.

[28] M. Harounabadi, D. M. Soleymani, S. Bhadauria, M. Leyh, and E. Roth-Mandutz, "V2X in 3GPP standardization: NR sidelink in release-16 and beyond," *IEEE Commun. Standards Mag.*, vol. 5, no. 1, pp. 12–21, Mar. 2021.

[29] M. H. C. Garcia et al., "A tutorial on 5G NR V2X communications," *IEEE Commun. Surveys Tuts.*, vol. 23, no. 3, pp. 1972–2026, 3rd Quart., 2021.

[30] *Study on Enhancement of 3GPP Support for 5G V2X Services; Release 16*, document TR 22.886 V16.2.0, 3GPP, Dec. 2018.

[31] *Technical Specification Group Services and System Aspects. Enhancement of 3GPP Support for V2X Scenarios. Release 15*, document TR 22.186, V16.2.0, 3GPP, Jun. 2019.

[32] *5G Automotive Association (5GAA)—C-V2X Use Cases Methodology, Examples and Service Level Requirements*, 5GAA, Munich, Germany, Jul. 2019.

[33] S. Gezici, "A survey on wireless position estimation," *Wireless Pers. Commun.*, vol. 44, no. 3, pp. 263–282, Feb. 2008.

[34] W. Zhuang, X. S. Shen, and Q. Bi, "Ultra-wideband wireless communications," *Wireless Commun. Mobile Comput.*, vol. 3, no. 6, pp. 663–685, 2003. [Online]. Available: https://onlinelibrary.wiley.com/doi/abs/10.1002/wcm.149

[35] D. Dardari, A. Conti, U. Ferner, A. Giorgetti, and M. Z. Win, "Ranging with ultrawide bandwidth signals in multipath environments," *Proc. IEEE*, vol. 97, no. 2, pp. 404–426, Feb. 2009.

[36] A. Conti, M. Guerra, D. Dardari, N. Decarli, and M. Z. Win, "Network experimentation for cooperative localization," *IEEE J. Sel. Areas Commun.*, vol. 30, no. 2, pp. 467–475, Feb. 2012.

[37] H. Wymeersch, J. Lien, and M. Z. Win, "Cooperative localization in wireless networks," *Proc. IEEE*, vol. 97, no. 2, pp. 427–450, Feb. 2009.

[38] D. Dardari et al., "High-accuracy tracking using ultrawideband signals for enhanced safety of cyclists," *Mobile Inf. Syst.*, vol. 2017, pp. 8149348:1–8149348:13, Mar. 2017.

[39] Y. Ge, M. Stark, M. F. Keskin, F. Hofmann, T. Hansen, and H. Wymeersch, "Analysis of V2X sidelink positioning in sub-6 GHz," 2022, *arXiv:2210.15534*.

[40] B. Panzner, T. Sahin, and P. Keshavamurthy, "Coexistence of 5G sidelink communication and 5G sidelink positioning," in *Proc. Int. Symp. ELMAR*, Sep. 2022, pp. 77–80.

[41] Y. Lu et al., "Joint positioning and tracking via NR sidelink in 5G-empowered industrial IoT: Releasing the potential of V2X technology," 2021, *arXiv:2101.06003*.

[42] Y. Wu et al., "Cooperative localization with angular measurements and posterior linearization," in *Proc. IEEE Int. Conf. Commun. Workshops (ICC Workshops)*, Jun. 2020, pp. 1–6.
[43] N. Piperigkos, A. S. Lalos, K. Berberidis, and C. Anagnostopoulos, "Cooperative multi-modal localization in connected and autonomous vehicles," in *Proc. IEEE 3rd Connected Automated Vehicles Symp. (CAVS)*, Nov. 2020, pp. 1–5.
[44] N. Piperigkos, A. S. Lalos, and K. Berberidis, "Graph Laplacian diffusion localization of connected and automated vehicles," *IEEE Trans. Intell. Transp. Syst.*, vol. 23, no. 8, pp. 12176–12190, Aug. 2022.
[45] K. Ansari, "Cooperative position prediction: Beyond vehicle-to-vehicle relative positioning," *IEEE Trans. Intell. Transp. Syst.*, vol. 21, no. 3, pp. 1121–1130, Mar. 2020.
[46] A. Kakkavas, M. H. C. Garcia, R. A. Stirling-Gallacher, and J. A. Nossek, "Multi-array 5G V2V relative positioning: Performance bounds," in *Proc. IEEE Global Commun. Conf. (GLOBECOM)*, Dec. 2018, pp. 206–212.
[47] S. M. Kay, *Fundamentals of Statistical Signal Processing, Volume 1: Estimation Theory* (Prentice-Hall Signal Processing Series), 1993.
[48] S. Zhang, T. Jost, R. Pöhlmann, A. Dammann, D. Shutin, and P. A. Hoeher, "Spherical wave positioning based on curvature of arrival by an antenna array," *IEEE Wireless Commun. Lett.*, vol. 8, no. 2, pp. 504–507, Apr. 2019.
[49] A. Guerra, F. Guidi, and D. Dardari, "Single-anchor localization and orientation performance limits using massive arrays: MIMO vs. beamforming," *IEEE Trans. Wireless Commun.*, vol. 17, no. 8, pp. 5241–5255, Aug. 2018.
[50] A. Kakkavas, M. H. C. García, R. A. Stirling-Gallacher, and J. A. Nossek, "Performance limits of single-anchor millimeter-wave positioning," *IEEE Trans. Wireless Commun.*, vol. 18, no. 11, pp. 5196–5210, Nov. 2019.
[51] A. Guerra, F. Guidi, D. Dardari, and P. M. Djuric, "Near-field tracking with large antenna arrays: Fundamental limits and practical algorithms," *IEEE Trans. Signal Process.*, vol. 69, pp. 5723–5738, Aug. 2021.
[52] A. Elzanaty, A. Guerra, F. Guidi, and M.-S. Alouini, "Reconfigurable intelligent surfaces for localization: Position and orientation error bounds," *IEEE Trans. Signal Process.*, vol. 69, pp. 5386–5402, 2021.
[53] H. L. Van Trees, *Optimum Array Processing: Part IV of Detection, Estimation, and Modulation Theory*. Hoboken, NJ, USA: Wiley, 2002.
[54] M. Rahal, B. Denis, K. Keykhosravi, M. F. Keskin, B. Uguen, and H. Wymeersch, "Constrained RIS phase profile optimization and time sharing for near-field localization," in *Proc. IEEE 95th Veh. Technol. Conf. (VTC-Spring)*, Jun. 2022, pp. 1–6.
[55] N. Cordeschi, D. Amendola, and E. Baccarelli, "Reliable adaptive resource management for cognitive cloud vehicular networks," *IEEE Trans. Veh. Technol.*, vol. 64, no. 6, pp. 2528–2537, Jun. 2015.
[56] V. Todisco, S. Bartoletti, C. Campolo, A. Molinaro, A. O. Berthet, and A. Bazzi, "Performance analysis of sidelink 5G-V2X mode 2 through an open-source simulator," *IEEE Access*, vol. 9, pp. 145648–145661, Oct. 2021.
[57] *Technical Specification Group Radio Access Network; Study on LTE-Based V2X Services; Release 14*, document TR 36.885, V14.0.0, 3GPP, Jul. 2016.

Nicolò Decarli (Member, IEEE) received the Ph.D. degree in electronics, telecommunications, and information technologies from the University of Bologna, Italy, in 2013. In 2012, he was a Visiting Student with the Wireless Communication and Network Sciences Laboratory, Massachusetts Institute of Technology, Cambridge, MA, USA. He is currently a Researcher with the Institute of Electronics, Computer, and Telecommunication Engineering (IEIIT), National Research Council of Italy (CNR). His research interests include wireless communication theory, radio localization, ultra-wide bandwidth systems, and radio frequency identification. In 2011, he served on the Local Organization Committee for the IEEE International Conference on Ultra-Wideband (ICUWB). He was the TPC Co-Chair of the 2018 IEEE ICC Workshop on Advances in Network Localization and Navigation (ANLN); and the Track-Chair of the 2018 IEEE International Symposium on Personal, Indoor, and Mobile Radio Communications (PIMRC).

Anna Guerra (Member, IEEE) received the Ph.D. degree in electronics, telecommunications, and information technologies from UNIBO in 2016.

From 2016 to 2021, she was a Post-Doctoral Researcher with the University of Bologna. Since 2021, she has been a Researcher with the National Research Council (CNR) of Italy. From 2018 to 2020, she received the Global Marie Skłodowska-Curie Research Fellowship for the H2020 AirSens Project. She spent the project's outgoing phase with Stony Brook University, Stony Brook, NY, USA. In 2023, she received the ERC Starting Grant for the project CUE-GO. She received the Best Student Paper Award at the 2014 IEEE International Conference on Ultra-Wideband held in Paris, France; and the Best Paper Award at the 2019 IEEE RFID-TA Conference, Pisa, and the 2021 IEEE International Conference on Autonomous Systems, Montreal, QC, Canada.

Caterina Giovannetti (Student Member, IEEE) received the M.S. degree (summa cum laude) in electronics and telecommunications engineering for energy from the University of Bologna, Italy, in 2022. Currently, she is a Research Fellow with the Institute of Electronics, Computer and Telecommunications Engineering (IEIIT), National Research Council (CNR) of Italy and affiliated with CNIT/WiLab.

Francesco Guidi (Member, IEEE) received the B.S. and M.S. degrees (summa cum laude) in biomedical engineering and in electronics and telecommunications engineering from the University of Bologna, Italy, in 2006 and 2009, respectively, and the joint Ph.D. degree in electronics, telecommunications and information technologies from École Polytechnique ParisTech, France, and the University of Bologna, in 2013. He is currently a Researcher with IEIIT-CNR, Italy. From 2015 to 2017, he was a recipient of an individual European Marie Skłodowska-Curie Fellowship at French Atomic Energy Commission (CEA-LETI), Grenoble, France. In 2019, he was a Visiting Scholar with Stony Brook University, New York, USA.

Barbara M. Masini (Senior Member, IEEE) received the Laurea degree (summa cum laude) in telecommunications engineering and the Ph.D. degree in electronic, computer science, and telecommunication engineering from the University of Bologna, Italy, in 2001 and 2005, respectively. She is currently a Senior Researcher with the Institute for Electronics and for Information and Telecommunications Engineering, National Research Council (CNR); and an Adjunct Professor with the University of Bologna. She works in the area of wireless communication systems. Her research interests are mainly focused on connected vehicles, from physical and MAC levels aspects up to applications and field trial implementations. Her research is also focused on relay assisted communications, energy harvesting, and visible light communication. She is responsible for a number of national and international projects on vehicular communications and urban intelligence. She is an Editor of IEEE ACCESS and *Computer Communication* (Elsevier).

Open Access funding provided by 'Consiglio Nazionale delle Ricerche-CARI-CARE-ITALY' within the CRUI CARE Agreement